The BGO Calorimeter of BGO-OD Experiment

To cite this article: B Bantes *et al* 2015 *J. Phys.: Conf. Ser.* **587** 012042

View the article online for updates and enhancements.

The BGO Calorimeter of BGO-OD Experiment

B. Bantes [1]**, D. Bayadilov** [2]**, R. Beck** [2]**, M. Becker** [2]**, A. Bella** [1]**,
P. Bielefeldt** [1]**, J. Bieling** [1]**, M. Bleckwenn** [1]**, S. Böse** [2]**, A. Braghieri** [3]**,
K.-Th. Brinkmann** [4]**, D. Burdeynyi** [5]**, F. Curciarello** [6,7]**, V. De Leo** [6,7,*]**,
R. Di Salvo** [8]**, H. Dutz** [1]**, D. Elsner** [1]**, A. Fantini** [8,9]**, O. Freyermuth** [1]**,
S. Friedrich** [4]**, F. Frommberger** [1]**, V. Ganenko** [5]**, D. Geffers** [1]**,
G. Gervino** [10,11]**, F. Ghio** [12,13]**, G. Giardina** [6,7]**, B. Girolami** [12,13]**,
D. Glazier** [14]**, S. Goertz** [1]**, A. Gridnev** [15]**, E. Gutz** [4]**, D. Hammann** [1]**,
J. Hannappel** [1]**, P.-F. Hartmann** [1]**, W. Hillert** [1]**, A. Ignatov** [16]**,
R. Jahn** [2]**, R. Joosten** [2]**, T.C. Jude** [1]**, F. Klein** [1]**, K. Koop** [2]**,
B. Krusche** [17]**, A. Lapik** [16]**, P. Levi Sandri** [18]**, I. Lopatin** [15]**,
G. Mandaglio** [6,7]**, P. Mei** [1]**, F. Messi** [1]**, R. Messi** [8,9]**, V. Metag** [4]**,
D. Moricciani** [8]**, M. Nanova** [4]**, V. Nedorezov** [16]**, D. Novinskiy** [15]**,
P. Pedroni** [3]**, M. Romaniuk** [8]**, T. Rostomyan** [17]**, N. Rudnev** [16]**,
C. Schaerf** [8,9]**, G. Scheluchin** [1]**, H. Schmieden** [1]**, V. Sumachev** [15]**,
V. Tarakanov** [15]**, V. Vegna** [1]**, D. Walther** [2]**, D. Watts** [14]**,
H.-G. Zaunick** [2]**, T. Zimmermann** [1]

[1] Universität Bonn, Physikalisches Institut, Nußallee 12, Bonn, D-53115, Germany
[2] Helmholtz-Institut für Strahlen- und Kernphysik, Nußallee 14-16, Bonn, D-53115, Germany
[3] INFN, sezione di Pavia, Via Agostino Bassi 6, Pavia, 27100, Italy
[4] Justus-Liebig-Universität Gießen, II. Physikalisches Institut, Heinrich-Buff-Ring 16, Gießen,
D-35392, Germany
[5] National Science Center, Kharkov Institute of Physics and Technology, Akademicheskaya St.
1, Kharkov, 61108, Ukraine
[6] INFN, sezione di Catania, via Santa Sofia 64, Catania, 95123, Italy
[7] Università degli Studi di Messina, Dipartimento di Fisica e di Scienze della Terra, v.le F.
Stagno d'Alcontres 31, Messina, 98166, Italy
[8] INFN, Roma Tor Vergata, Via della Ricerca Scientifica 1, Roma, 00133, Italy
[9] Università di Roma "Tor Vergata", Dipartimento di Fisica, Via della Ricerca Scientifica 1,
Roma, 00133, Italy
[10] INFN, sezione di Torino, Via P.Giuria 1, Torino, 10125, Italy
[11] Dipartimento di Fisica, Università di Torino, via P. Giuria 1, 10125, Torino, Italy
[12] INFN, sezione di Roma, c/o Dipartimento di Fisica - Università degli Studi di Roma "La
Sapienza" P.le Aldo Moro 2, Roma, 00185, Italy
[13] Istituto Superiore di Sanità, Viale Regina Elena 299, Roma, 00161, Italy
[14] The University of Edinburgh, James Clerk Maxwell Building, Mayfield Road, Edinburgh
EH9 3JZ, United Kingdom
[15] Petersburg Nuclear Physics Institute, Gatchina, Leningrad District, 188300, Russia
[16] Russian Academy of Sciences Institute for Nuclear Research, prospekt 60-letiya Oktyabrya
7a, Moscow 117312, Russia
[17] Institut für Physik, Klingelbergstrasse 82, Basel, CH-4056, Switzerland
[18] INFN - LNF, Via E. Fermi 40, Frascati, 00044, Italy

E-mail: `vdeleo@unime.it`

Abstract. The BGO Rugby Ball is a large solid angle electromagnetic calorimeter now

installed in the ELSA Facility in Bonn. The BGO is operating in the BGO-OD experiment aiming to study meson photoproduction off proton and neutron induced by a Bremsstrahlung polarized gamma beam of energies from 0.2 to 3.2 GeV and an intensity of 5×10^7 photons per second. The scintillating material characteristics and the photomultiplier read-out make this detector particularly suited for the detection of medium energy photons and electrons with very good energy resolution. The detector has been equipped with a new electronics read-out system, consisting of 30 sampling ADC Wie-Ne-R modules which perform the off-line reconstruction of the signal start-time allowing for a good timing resolution. Performances in linearity, resolution and time response have been carefully tested at the Beam Test Facility of the INFN National Laboratories in Frascati by using a matrix of 7 BGO crystals coupled to photomultipliers and equipped with the Wie-Ne-R sampling ADCs.
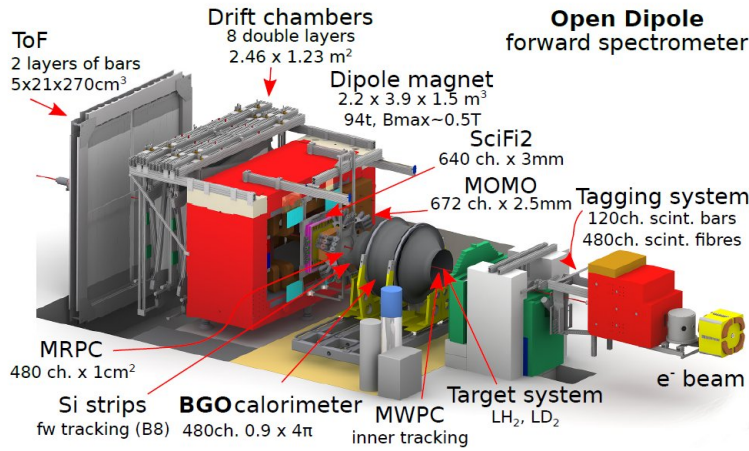
1. Introduction

A detailed and precise knowledge of the nucleon spectroscopy is undoubtedly one of the cornerstones for our understanding of the strong interaction in the non-perturbative regime. Todays privileged way to get information on the excited states of the nucleon is the meson photo- and electroproduction[1]. The attempt is to extract, from the phoproduction, the electromagnetic couplings and furthermore the hadronic properties of the excited nucleon states that cannot be accessed via pion scattering, either because the resonances largely overlap, or because of a weak coupling to the single pion-nucleon channel. Polarization degrees of freedom in photoproduction processes play a crucial role. Polarization observables arising from interference mechanisms, are highly sensitive to the details of the interaction revealing resonance properties that are difficult to extract from a cross-section measurement, where a single contribution often dominates[2]. The corresponding database has considerably expanded over the last years thanks to a combined effort of dedicated facilities worldwide. Not only did the recent experiments brought a quantitative improvement by measuring cross-sections with unprecedented precision for a large number of channels but they also allowed a qualitative leap by providing high-quality data on polarization observables.

The BGO-OD experiment at the ELSA facility in Bonn involves the use of a Bremsstrahlung tagged and polarized photon beam of energy between 0.2 and 3.2 GeV, a large solid angle high resolution BGO calorimeter combined with the plastic scintillator barrel and two Multi-Wires Proportional Chambers (MWPC) and the Open Dipole spectrometer equipped with tracking detectors. This apparatus will be used to measure polarization observables and cross sections in the photoproduction of pseudo-scalar and vector mesons off a Hydrogen or Deuterium target.

2. Experimental apparatus at BGO-OD

The BGO-OD apparatus is composed of two main parts: a central detector system and a forward spectrometer for charged particles, completed by a photon tagging system. The tagger, consisting of 120 channels, will cover the energy range $(0.1 \div 0.9)E_{e-}$ with variable resolution $(10 \div 40 \text{ MeV})$[3]. It is designed to handle a high intensity beam (up to $5 \cdot 10^7 s^{-1}$). One of the central detectors of the experimental setup is the high energy resolution and large solid angle (0.9 π) BGO electromagnetic calorimeter that will be described in detail later. The calorimeter is combined with two multi-wire proportional chambers (MWPC) for inner tracking and a plastic scintillator barrel for particle identification through the measurement of dE/dx. The region between the acceptance of the central detector and the forward spectrometer will be covered by an azimuthally symmetric Multi-gap Resistive Plate Chamber (MRPC) detector.

The forward spectrometer is based on a large open dipole magnet that uses a dipolar field of about 0.5 T for the separation, identification and measurement of the momentum (3% resolution) of charged particles emitted in the photoproduction processes. For this purpose, the
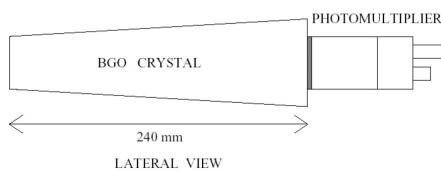
Figure 1. BGO-OD experimental apparatus.

spectrometer is equipped with MOMO and SciFi2 detectors, eight double layer drift chambers (DCs) and a time-of-flight (TOF) detector [3]. The two fiber hodoscopes MOMO and SciFi2, located in front of the magnet, allow the tracks reconstruction before the curvature caused by the magnetic field. Behind the magnet, tracking is done by a set of 8 double layer drift chambers in four different orientations, vertical wires to measure the x -coordinate, horizontal for the the y -coordinate, and tilted by 9 from vertical, for a u - and v -coordinate. The forward spectrometer is completed by a set of time-of-flight walls that are used for charged particle identification in combination with the momentum reconstruction provided by the tracking detectors[4].
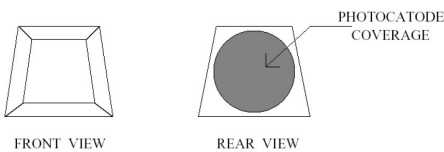
3. The BGO calorimeter
The calorimeter is designed to study photonuclear reactions up to about 2 GeV, in particular exclusive channels where neutral products (γ and neutral mesons decaying in two or more photons, as π, η, η', K^0, ϕ) and charged particles (detectable to some extent) are emitted[5].

Figure 2. Schematic views of a BGO crystal.
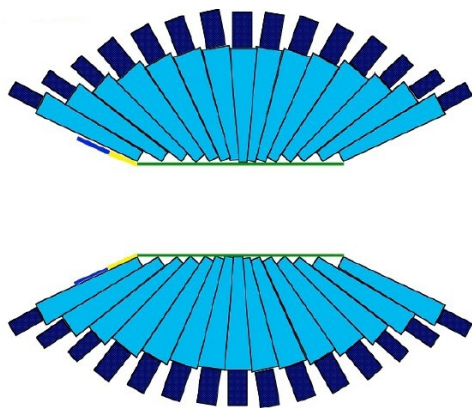

Figure 3. BGO crystal coupled to the photomultiplier.

Figure 4. Schematic views of a BGO crystal.

The features of the apparatus are a large solid angle (0.9π), extended granularity, good

detection efficiency for neutral products and also a good energy resolution to low momentum (<0.8 GeV/c) protons. Moreover, the high density, the short radiation length ($X_0 = 1.12$ cm), the high atomic number made this inorganic scintillating material ($Bi_4(GeO_4)_3$) particularly suited for the construction of an electromagnetic calorimeter with limited sizes. The crystal is not hygroscopic and the wavelength range of the emitted light (480 nm) can be easily matched with standard photomultipliers. The calorimeter is composed of 480 BGO crystals. The crystals are of 8 different dimensions and are shaped like pyramidal sectors with trapezoidal bases. They define 15 angular regions (θ) in the plane containing the symmetry axis of the calorimeter, coincident with the beam axis, and 32 (ϕ) in the plane orthogonal to the beam axis[6]. The 480 crystals have all the same length of 24 cm ($\simeq 21$ radiation lengths), for a good confinement of photon showers in the GeV region, and are arranged in such a way that the reaction products encounter the same thickness of BGO. Each crystal is wrapped up in a thin (30 μm) aluminized mylar reflector, and its back side is optically coupled to a photomultiplier (PM). The crystals have been treated by the manufacturer in order to guarantee a uniformity in the light collection along the crystal length better than at least 95% (it is even better than 98% for some crystals) and this will represent a deterioration of the energy resolution by a constant term of the order of 0.3%[6].
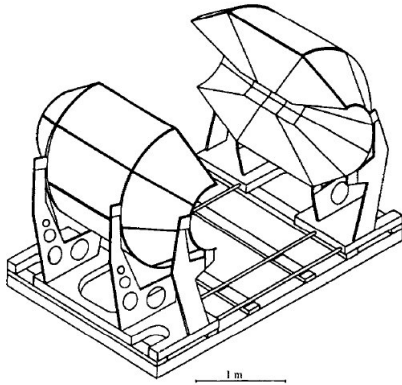

Figure 5. Scheme of the BGO sectors. The crystals cover the polar angle between 25° and 155° in the laboratory reference frame (15 sectors), while the azimuthal angle is totally covered (32 sectors).
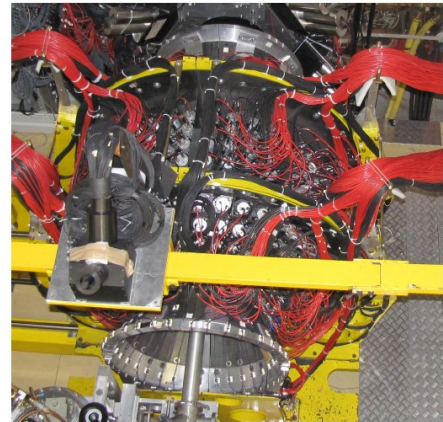
The mechanical support structure consists of 24 baskets of Carbon fiber composite material supported by an external steel frame. Each basket is divided into 20 cells with very thin walls, 0.38 mm for the inner and 0.54 mm for the outer walls, to keep the crystals optically and mechanically separated. The Carbon fiber has been preferred to other materials like Aluminum for its higher rigidity and lower gamma ray attenuation due to its low Z number. The support frame is divided into two halves which can be taken apart by 1.5 m to allow access to the target and central detector region. When closed the structure leaves a 20 cm diameter hole along the beam-line for the insertion of the target, the cylindrical wire chambers and the plastic scintillator barrel[5].

4. BGO readout system and calibration procedure
The BGO acquisition is performed by using thirty Wiener Sampling ADC modules. The ADC modules AVM16-Mambo operate with a sampling frequency of 160 MHz (corresponding to 6.25 ns interval between two samples) with 12 bit resolution (i.e. 4096 channels). The signal is sampled inside a time interval defined by the user, that can start after or before the trigger signal. The AVM16 modules have 16 channels and one trigger input but they are provided also of an internal trigger (level trigger). We use this option for calibration purposes. The modules allow the extraction of the main parameters of the pulse as the total and partial integrals of the signal, amplitude and time of relative maxima and minima and the start time of the signal.
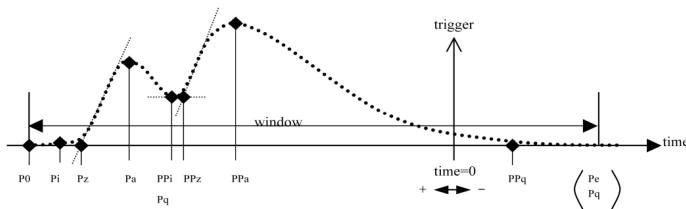
Figure 6. Sketch of the BGO calorimeter showing the carbon fiber baskets mounted on the external support frame separable into two halves.
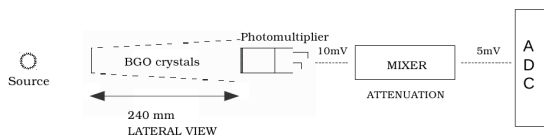

Figure 7. Top view of the BGO Calorimeter.

An example of the main features for a signal with pile-up events is illustrated in the figure 8: the window start point (P0), which represents the user defined latency time; amplitude and time of minima (Pi, Ppi, ...) and maxima (Pa, Ppa, ...), extracted when a rising slope is detected; the pulse start time (Pz, Ppz, ...), extrapolated from the crossing of the slope and the pedestal value (or the current pedestal value for pile-up signals) and the total and partial charge integrals (Pq, Ppq).

Figure 8. Feature extraction parameters.

The absolute calibration of the Bgo Rugby Ball is performed by using the more energetic photons (1.275 MeV) emitted by three ^{22}Na sources located inside the BGO cylindrical hole. The equalization of the response of the 480 crystals is obtained by setting all the photomultiplier (PM) gains varying their high voltages.
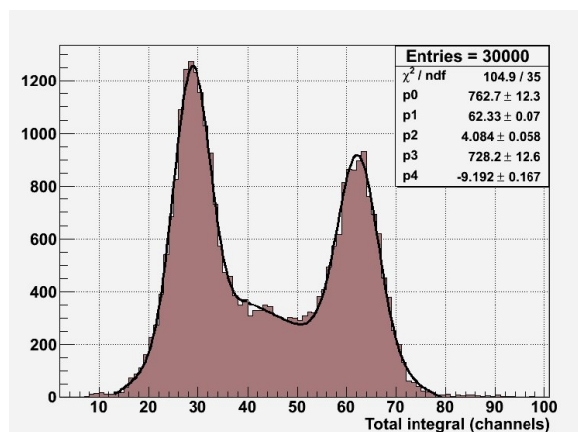

Figure 9. Scheme of the electronic chain used for the calibration procedure.

This procedure is strictly necessary, because a threshold on the hardware sum of the energy released in the BGO is used as a trigger for the experiment. After the equalization, for the same energy released, the response of the PM associated to each crystal will be located at the same ADC channel. For the calibration procedure an internal trigger which is provided by the ADC, when a signal overcomes a certain threshold, was used; it was chosen in order to guarantee the

same statistics on all the crystals, which a global trigger on the hardware sum of the energies of all the crystals could not insure. In Figure 9 a schematic representation of the experimental chain of calibration is shown: the output signal from the phototube, coupled to the crystal, is sent to a mixer that delays, in case attenuates, splits the signals into two parts, one sent to the ADC for the readout and the other to the sum over the signals. To obtain the calibration constants for each channel, we fix the PM voltages so that the response to the energy of the second peak of the source is located at the channel 60 of the ADCs. The channel is fixed within a tolerance of $\pm 3\%$, which, in any case, does not affect the calibration of the data, since the calibration constant of each crystal is registered and used for the offline energy conversion[7]. It is necessary to repeat the calibration procedure two times per day because the calibration constants of each crystal may change during time. The reasons are essentially two: variation in the crystal light output due to temperature effects and variation in the PM gain. Gain variations of the photomultipliers may occur as a consequence of the following effects[5]:

-photocathode temperature variation;

-instability in the high voltage power supply;

-aging of the cathode and dynode materials;

-voltage dividers instability.

In figure 10, a typical BGO calibration spectra acquired with the AVM-16 ADC modules is represented, where both the peaks of the ^{22}Na source are visible.

Figure 10. BGO calibration spectrum where the two peaks of the ^{22}Na source are visible.

5. Performances of the BGO calorimeter

The linearity and resolution in the energy reconstruction and the performances in the time response of the BGO crystals in combination with the new readout system (AVM16 ADC modules) have been recently studied at the BTF (Beam Test Facility) in Frascati.
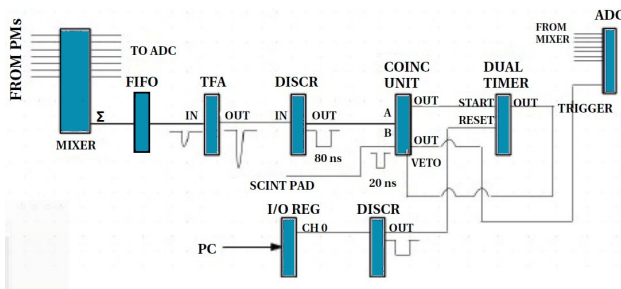
The BTF is part of the DAΦNE ϕ-factory complex which includes a high current electron and positron LINAC, a 510 MeV e^- and e^+ accumulator and two 510 MeV storage rings[8]. Before the high-intensity electron or positron beam pulses produced by the 60 m long LINAC are injected into the double storage ring, they can be extracted to a transfer line that is dedicated to the calibration of particle detectors (the BTF transfer line). Here, the number of particles can be reduced to a single electron per pulse by means of a variable thickness copper target. Moreover, a dipole magnet and a system of slits, located before and after the dipole, allow the selection of a particular energy of the beam and its collimation. In this way, it is possible to keep under control not only the energy of the beam but also the number of electrons that enter in the experimental area (the multiplicity), allowing to reach energy values up to 2-3 GeV when several electrons simultaneously impinge on the detector.

During the test we used 7 BGO crystals arranged as a matrix inside a PVC basket with removable walls. The position of the walls could be adjusted with Aluminum screws in order to guarantee a better tightness among the crystals. No inert material was present between them because they were not mechanically separated.

The trigger to the acquisition has been provided by a plastic scintillator plate, located in front of the crystals, when the signal is in coincidence with an over threshold deposited energy in the BGO crystals.

5.1. Electronics readout

A scheme of the electronics readout used during the tests is shown in the figure 11. Here, the signal coming from the PM of each crystal was split and attenuated and sent to the ADC module for digitization, or sent to a linear Fan-In-Fan-out together with the signals coming from the other crystals for trigger purposes. The linear sum of the seven signals was amplified and sent to a threshold discriminator and then to a coincidence unit, together with the discriminated signal of the scintillator pad. A veto to the coincidence unit, to avoid further triggers during the dead time of the acquisition, is provided by a Dual Timer module activated by an output of the coincidence unit.
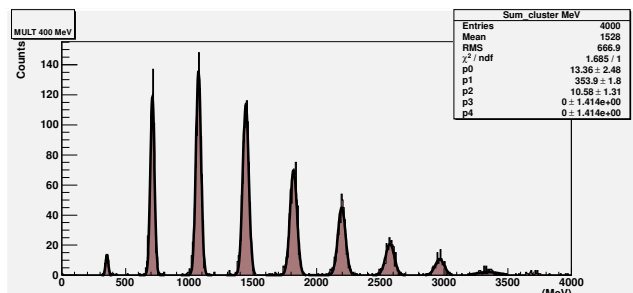

Figure 11. The electronics scheme of the crystals read-out: signals from the BGO are split and (i) attenuated and sent to the ADC module or (ii) summed with the other signals, amplified and discriminated for trigger purposes.

The reset of the Dual Timer is externally provided by the acquisition program via an I/O-Register.

5.2. Analysis and results

We collected data at six different settings of the beam energy with different multiplicity values: 100 MeV (4 peaks of multiplicity=1÷4), 150 MeV (6 peaks), 200 MeV (7 peaks), 300 MeV (7 peaks), 400 MeV (9 peaks) and 500 MeV (4 peaks). For each event, we considered a cluster of all the crystals, summing up the energies deposited in all of them, since the e.m. shower spreads over several crystals.

Figure 12. Energy spectrum of the beam when the single electron has an energy of $400\,MeV$. The visible peaks correspond to the different value of multiplicity of electrons, i.e. correspond the energies which are multiple of E_{NOM} (E_{NOM}, $2E_{NOM}$, ... nE_{NOM}).
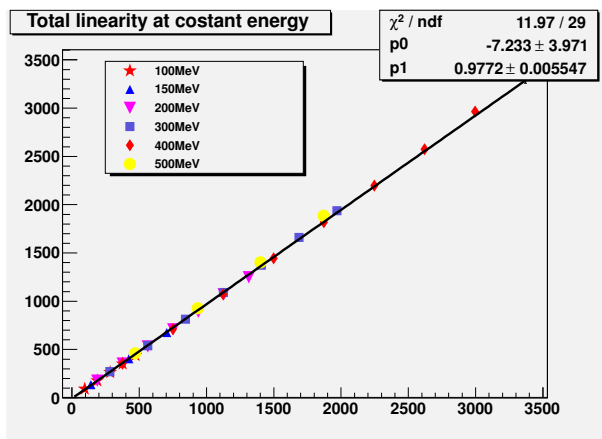
The energy spectrum of the beam for the energy setting of 400 MeV is shown in figure 12. The peaks correspond to the different values of multiplicity of electrons and then correspond to

the energies which are multiple of E_{NOM} (E_{NOM}, $2E_{NOM}$, ... nE_{NOM}).

As one can see, the distributions are well distinguished so they have been fitted with a gaussian function (plus a background approximated with a straight line) with mean value of the energy E_{meas} and resolution $\sigma_{E_{meas}}$.

Thus, it was possible to extract the linearity curve of the detector plotting the mean value of the energy E_{meas} as a function of the nominal energy E_{NOM}.

Figure 13. Linearity curve of the detector: the mean value of the energy (E_{meas}) obtained from the fit is plotted as a function of the nominal energy (E_{NOM}). The error bars correspond to the resolution σ of the gaussian fit. Points of the same colour refer to the data of the same energy setting with increasing value of multiplicity.

In figure 13 we reported the fitted values of the energy with the error coming from the fitted resolution as a function of the nominal energy for all energy settings and multiplicities. Points of the same colour refer to the data of the same energy setting with increasing value of multiplicity.

They follow a linear behaviour:

$$E_{meas} = p_0 + p_1 * E_{nom} \tag{1}$$

with

$p_0 = (-7.233 \pm 3.971) MeV$

$p_1 = -0.977 \pm 0.0055 MeV$

and a satisfactory reduced χ^2_{red} value: $\chi^2_{red} = 0.4$. Only the three points at the highest energies, 2400MeV, 2800 MeV, and 3200 MeV (corresponding to 6,7 or 8 electrons of energy 400MeV each) are slightly higher than expected, probably denoting small non-linearities in the PM of the central crystal of the matrix or of the ADC module.

The linearity curve was extracted also plotting the fitted vs. the nominal energy for the different multiplicities (up to four) at each energy setting in order to see if differences arise with the previous case.
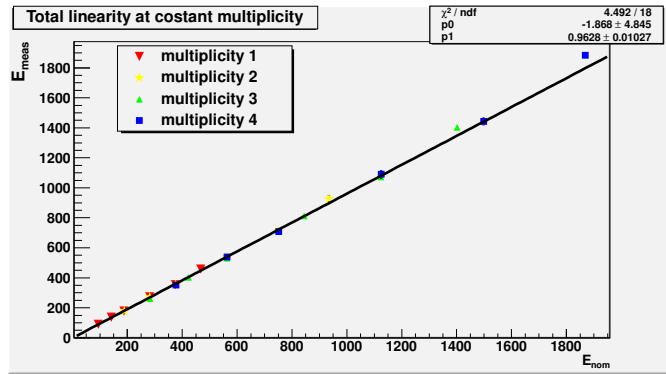
Since the calorimeter is a linear device, we expect that if a single electron of energy E_0 deposits its energy in the detector or n electrons each of energy $E_i = E_0/n$, the response of the detector should be essentially the same in the two cases.

We compared the two results and we found that they are in good agreement. In the last case the fit provides a lower value of the χ^2_{red} (0.25) and:

$p_0 = (-1.868 \pm 4.845) MeV$

$p_1 = 0.9628 \pm 0.01027$

because we have not considered the peaks of higher multiplicity that are characterized by a greater spread.

Figure 14. Linearity curve of the detector: the mean value of the energy (E_{meas}) obtained from the fit is plotted as a function of the nominal energy (E_{NOM}). The error bars correspond to the sigma of the gaussian fit. Only data for multiplicities less or equal four are reported and points with the same colour represent data obtained at the same multiplicity.

The BGO resolution in combination with the new ADC module, was extracted subtracting the BTF resolution, which is $\simeq 1\%$(RMS) at all the energies, from the measured resolution:

$$(\sigma_{BGO})^2 = (\sigma_{meas})^2 - (\sigma_{BTF})^2 \tag{2}$$

The energy resolution was parameterized in the usual way:

$$\frac{\sigma}{E}(\%) = a_{CONST} \oplus \frac{a_{STAT}}{\sqrt{E_{NOM}}} \oplus \frac{a_{NOISE}}{E_{NOM}} \tag{3}$$
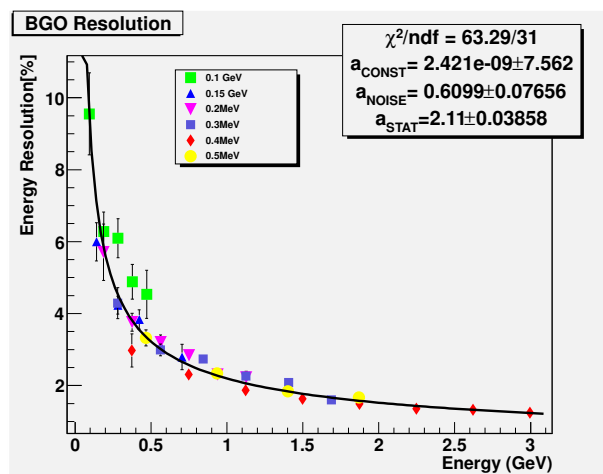
where the terms are summed in quadrature.

The first term, a_{CONST} is the constant term. It gives the asymptotic behaviour and it is connected to the intercalibration precision. It is related also to the longitudinal non-uniformities ($\simeq 0.3\%$) in the collection of the emitted light and to the temperature fluctuations.

The second term, a_{STAT} is the statistical term. It containes sampling and fluctuations of all kinds.

The last term, a_{NOISE} is generally negligible at high energies and it is connected to the electronic noise.

The data were fitted according to the previous formula and the result of the fit is displayed in figure 15.
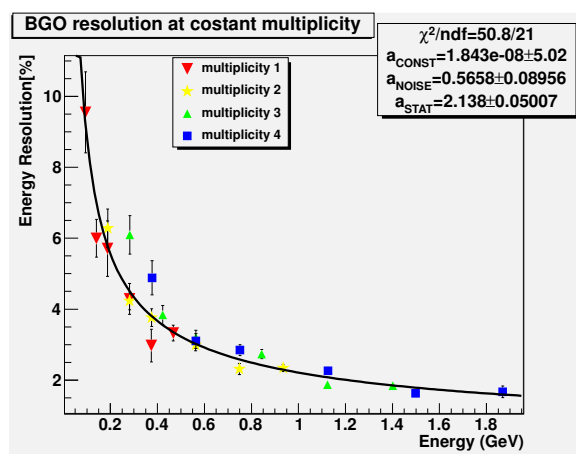

Figure 15. The BGO energy resolution, extracted from the fit of the peaks with a gaussian distribution and subtracted of the BTF energy resolution, as a function of the nominal energy. Data for all energy settings and multiplicities are reported and points with the same colour represent data obtained at the same energy settings.

We can see that:

- the constant term a_{CONST} is resulted about zero. Probably the reason is that the data taking was very near in time to the equalization procedure, so the fluctuations in calibrations are negligible as well as the fluctuations in temperature. Another possible reason is that we are overestimating the BTF resolution.

- a_{STAT} is reasonable and comparable with other published results[9].

- a_{NOISE} is small as it could be expected from read-out devices such as the photomultipliers.

As before, we have compared the energy resolutions concerning energies obtained in different ways (one single electron with energy E_0 or n electrons with energies E_0/n) and we found reasonable agreement between the different cases. Data of the same colour represent the results obtained at the same multiplicity for different energy settings.

Figure 16. The BGO energy resolution, extracted from the fit of the peaks with a gaussian distribution and subtracted of the BTF energy resolution, as a function of the nominal energy. Only data for multiplicities less or equal four are reported and points with the same colour represent data obtained at the same multiplicity.
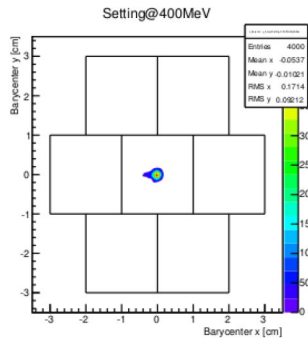
We have not observed clear difference with respect to the simplest case of one single electron. However, as it's possible to see from the plot 15, the better fit is given from the energy setting of $400 MeV$. The fact has an explanation. In fact, studying the spot of the beam has been found that only in the case of this energy setting the beam was perfectly centered and above all, it has a spread lower than the other settings of energy. In the figure 17 the spatial distribution of the beam, overlapped to the matrix of the seven crystals, is shown for the energy settings of 400 MeV and 500 MeV.

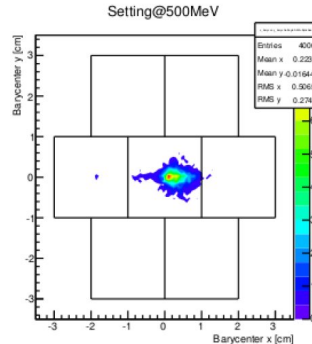### 5.3. Time response of the detector

For the first time the time response of the detector has been studied with a test beam and its time resolution has been estimated. In figure 19, the distribution of the start time for a central and a lateral crystal of the BGO matrix is illustrated.

As it is possible to see from the figure 19 for a central crystal (as the crystal number 3) we have a typical time resolution less than $3ns$; for a lateral crystal (as the crystal number 0) the measured resolution is about $6-8ns$. The reason for the different measured resolution is that since the crystal number three received much more energy than the other ones, most of the times the acquisition has been triggered by this crystal.
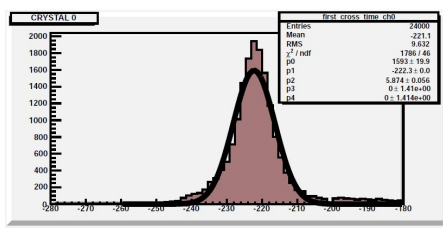
A difference in typical mean value is visible between the large and the small crystals: in the first case the t_{lrg} is about $-234ns$, instead in the second case the t_{sml} is about $-222ns$ with a $\Delta t \simeq 10-12ns$ and $|t_{lrg}| > |t_{sml}|$. The different electron transit time in the photomultipliers of different sizes is the explanation for the Δt.
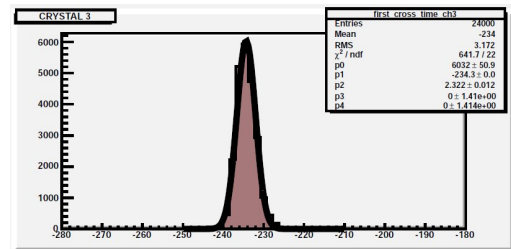
Figure 17. Bidimensional distribution of the x and y coordinates of the centroid for the energy setting of 400 MeV.

Figure 18. Bidimensional distribution of the x and y coordinates of the centroid for the energy setting of 500 MeV.

Figure 19. The start time distribution of a lateral crystal of the matrix. Distributions has been fitted with a gaussian; the fit parameters are reported in the plot.

Figure 20. The start time distribution of a central crystal of the matrix. Distributions has been fitted with a gaussian; the fit parameters are reported in the plot.
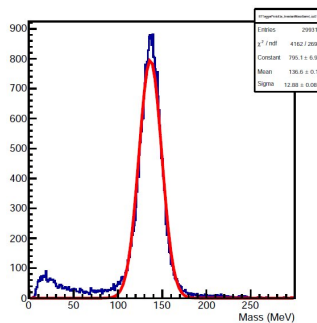
6. Some preliminary results at BGO-OD

The good status of the BGO calorimeter allows the invariant mass reconstruction of the π^0 meson and the missing mass from two gammas that are visible in the figures 21 and 22.

They have been obtained by using the geometrical coincidence between the BGO calorimeter and the barrel scintillator.
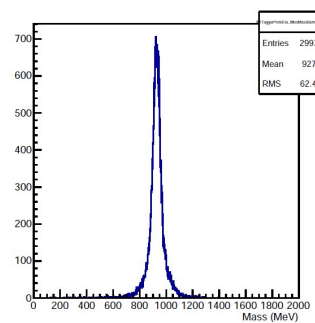
7. Conclusions

The BGO calorimeter operating in the BGO-OD experiment has been described. We reported the calibration procedure of the BGO calorimeter that we used.

The performances of the detector in combination with the new readout system of AVM16 Sampling ADC modules have been studied at the BTF of Frascati. The global resolution of the BGO is confirmed to be about 3% at 1 GeV, which is compatible with the requests at the BGO-OD experiment. For the first time, we have studied the time response of the detector with a test beam and we have estimated its time resolution ($\sim$ 3ns (RMS)). The excellent status of the BGO Ball has allowed to obtain promising results during the beam time tests, as the reconstruction of the invariant mass of the π^0 meson and the missing mass from two gammas.

Figure 21. Invariant mass reconstruction of the π^0 meson from two gammas where the particle identification is obtained by using the geometrical coincidence between the BGO calorimeter and the barrel scintillator[10].

Figure 22. Missing mass reconstruction from two gammas where the particle identification is obtained by using the geometrical coincidence between the BGO calorimeter and the barrel scintillator[10].

References

[1] Lleres A et al. 2009 *Eur. Phys. J. A* **39** 149161
[2] Di Salvo R et al. 2009 *Eur. Phys. J. A* **42**, 151157
[3] http://bgo-od.physik.uni-bonn.de
[4] Levi Sandri P et al. 2013 *Int. J. Mod. Phys.* **26** 1460093
[5] Ghio F et al. 1998 *Nucl. Instr. and Meth. in Phys. Res. A* **404** 71-86
[6] Zucchiatti et al. 1992 *Nucl. Instr. and Meth. in Phys. Res. A* **317** 492-497
[7] De Leo V et al. 2013 *J. Phys.: Conf. Ser.* **424** 012008
[8] Mazzitelli G, Ghigo A, Sannibale F, Valente P and Vignola G 2003 *Nucl Instr. Meth. A* **515** 516.
[9] Kampert K -H et al. 1994 *Nucl. Instr. and Meth. A* **349** 81.
[10] Magnisi L 2014 Bachelor Thesis *Private Communication.*